

DETC2017-67222

## DESIGN OPTIMIZATION OF A PRISMATIC-REVOLUTE-REVOLUTE JOINT HAND FOR GRASPING FROM UNCONSTRAINED VEHICLES

**Spencer B Backus**  
Yale University  
New Haven, CT, USA

**Aaron M. Dollar**  
Yale University  
New Haven, CT, USA

### ABSTRACT

Adding grasping and manipulation capabilities to unconstrained vehicles such as UAVs, AUVs, and small space craft so that they can deliver cargo, grasp and retrieve objects, perch on features in the environment, and even manipulating their environment is an ongoing area of research. However, these efforts have relied heavily on structuring the interaction task and have predominantly utilized existing gripper designs that were not specialized for the platform or task. In this paper, we present a parametric model of a novel underactuated hand design that is composed of prismatic-revolute-revolute joint fingers. This kinematic configuration attempts to minimize disturbance forces to the body of the vehicle while achieving stable grasps on a wide range of objects under significant positional uncertainty. In particular, this paper investigates the impact of various design parameters, including the relative link lengths and force allocation across the three joints, on grasping performance and suggests optimal design parameters for a prototype hand.

### INTRODUCTION

Most grasping research has focused on static grasping, where the robot and object are not moving relative to each other. This research has resulted in the design of many different hands, ranging from simple single degree of freedom (DOF) parallel jaw grippers to high DOF anthropomorphic hands such as the Shadow and DLR hands [1, 2]. Between these extremes are many hand designs that utilize one or a few actuators and some combination of fully actuated, passive, and coupled or underactuated degrees of freedom [3-8].

Existing work on aerial grasping has primarily utilized helicopter and quad rotor based UAVs equipped with simple hands and has focused on grasping objects and vehicle perching [9, 10]. Researchers have attempted to tackle this problem at multiple levels including end effector design, vehicle design



**Figure 1. Example of a UAV preparing to grasp an object while in flight.**

and control, and robotic arm design and integration. They have also focused on a number of different applications including cargo transport, grasping from UAVs, perching, and using multi degree of freedom arms to increase the manipulation capabilities of UAVs. The simplest application has been cargo transport and these systems have relied on external mechanisms to load the vehicles [11-13]. More ambitious projects have attempted to build systems capable of grasping and perching but most have utilized specialized single purpose grippers that utilize various forms of adhesion such as magnetism, suction, dry adhesion, or microspines for attachment and therefore are limited in what they can grasp [14-21]. Some mechanical grippers have also been demonstrated for grasping and perching but these designs have either been very simple single purpose grippers or have been slightly modified versions of existing hands such as the example show in Figure 1 [22-31]. Lastly, several research groups have developed UAVs outfitted with multi degree of freedom robotic arms but these projects tend to focus on the control of the overall system and rely on very

simple grippers when performing grasping tasks [31-35].

However, there have been few concerted efforts to investigate or design general purpose grippers for aerial vehicles or other highly mobile and unstable platforms like AUVs and spacecraft. Therefore, in this paper we investigate a new hand design intended specifically for aerial grasping that is composed of three link prismatic, revolute, revolute (P-R-R) joint fingers. This kinematic configuration derives from insights from our previous modeling of hands for grasping and perching and development of a hand prototype with related kinematics [36, 37].

We begin by describing the overall kinematics and actuation scheme used in this hand design. We then describe the numerical model used to evaluate the hand's behavior as well as the metrics used to compare the effects of various design parameters on the hand's performance. Lastly, we present and discuss the results from a parametric investigation of the effect of the link lengths and joint moment arms and discuss their impact on the hand's performance.

## HAND DESIGN

We begin by describing the general configuration of the hand and the motivation for studying this particular kinematic configuration. Previous modeling of a two joint revolute finger hand showed the impact of palm spacing (the distance between the two proximal revolute joints) on grasp performance and how it related to object size [37]. Similarly, our experience with the performance of the Model S hand prototype demonstrated the utility of a hand that combines prismatic and revolute joints in series in each finger [36]. Building upon these results, in this paper we describe and analyze a hand that combines elements of multilink revolute and prismatic joint hands. It consists of opposed P-R-R joint underactuated fingers as shown in Figure 2. We believe that this combination of prismatic and revolute joints effectively adds a variable size palm to the hand, allowing it to adapt to the size of the object. However, unlike a purely prismatic joint hand, the addition of multilink revolute joint fingers increases the hand's ability to conform to objects and the strength of the resulting grasp. Lastly, actuation and control complexity can still be minimized by actuating all of the joints with a single actuator and underactuated transmission that exerts a force ( $F_T$ ) on the prismatic joint and proportional torques ( $\tau_1 = F_T R_1$ ,  $\tau_2 = F_T R_2$ ) about the revolute joints.

We also selected this hand morphology since aspects of its grasping behavior are desirable when grasping from a UAV. Unlike a purely revolute joint hand, the P-R-R joint kinematics and initial joint configuration of the fingers perpendicular to the palm ensure that fingertip motion is parallel to or towards the palm of the hand when grasping. This constraint on the fingertip trajectory means that contact forces on the grasped object arising from the closing motion of the hand will push the object further into the grasp, thereby reducing the chance of the hand inadvertently knocking the object out of the hand prior to the acquisition of a secure grasp. Similarly, this fingertip trajectory ensures that actuation of the hand will not result in unexpected contact with the environment that may push the

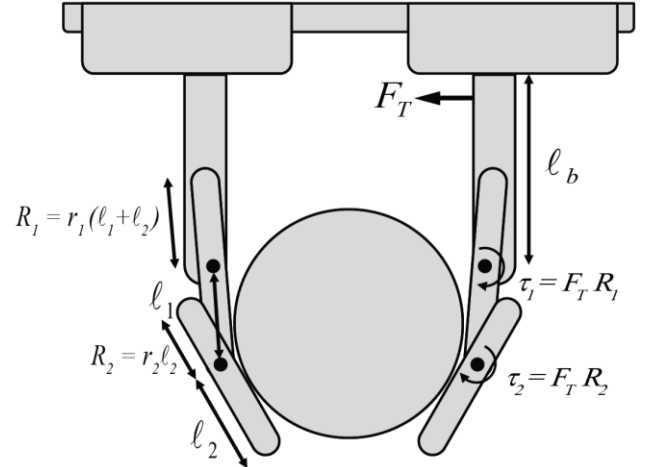


**Figure 2. Diagram of the proposed hand design grasping a circular object, labeled with important parameters.**

hand away from the desired position or generate unexpected normal reaction forces on the vehicle. Furthermore, the between finger coupling implemented in this design means that similar contact forces will be exerted on an object wherever it is positioned laterally in the hand's workspace and ensures that minimal force will be exerted on the object until both fingers make contact. This feature improves the hand's tolerance of positional error and minimizes the lateral reaction forces exerted on the vehicle during grasp acquisition. Lastly, the within finger underactuation allows the fingers to conform to the object after both fingers make contact, improving the robustness of the resulting grasp.

The variable palm width of the P-R-R hand morphology also contributes to the positional error tolerance of this design since it facilitates the initial pose of the hand consisting of widely spaced opposing fingers normal to the palm. This initial configuration of the hand ensures a large approach volume (defined as the convex polyhedron inscribed between the fingers and palm) and approach area (the polygon inscribed between the fingertips [38]) for a given palm width and finger length. The large approach area allows for large positional errors when approaching the object while the large grasp volume allows the object to be caged by the gripper prior to contact. In comparison, hand designs built with revolute joint fingers and a fixed palm width often have closely spaced proximal joints and widely opened fingers that results in a large approach area but small approach volume. This combination is undesirable when attempting to grasp with high positional error while still minimizing pre-grasp contact forces since objects may contact the palm before they are fully caged by the fingers.

## HAND KINEMATICS AND ACTUATION

In the remainder of this paper we focus on a 2D planar model of this hand design shown in Figure 2. The simulated hand is composed of two digits and each digit consists of a prismatic joint located in the palm of the hand followed by two revolute joints. The proximal phalanx of the finger extends from the prismatic joint to the first revolute joint and is

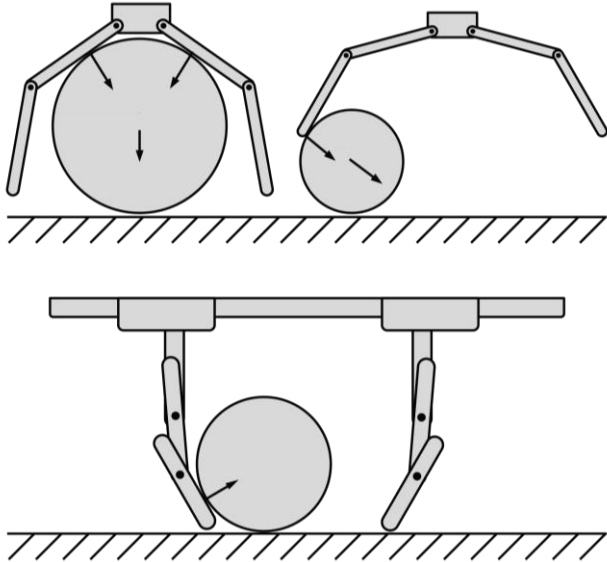


**Figure 3. Diagrams of the expected object contact force for a revolute joint hand (top) and the proposed design (bottom)**

perpendicular to the prismatic joint. The intermediate phalanx connects the first revolute joint to the second and the distal phalanx extends from the final joint to the fingertip. When fully extended against joint travel limits, all three phalanges are collinear and perpendicular to palm. The prismatic joints of the fingers are parallel and lie in the plane of the palm. The revolute joints axes of each finger are also parallel to the palm of the hand. Lastly, we assume that the fingers can interdigitate and achieve wrap grasps about objects.

Both fingers are underactuated; the flexion of the fingers is achieved by applying actuator force proportionally about each joint. Equal force is also applied to each finger, ensuring both between and within finger adaptability. Extension of the fingers is accomplished via individual return springs located in each joint.

## GRASP MODEL

Because a completely realistic physics based model of the hand's behavior and its interaction with an object is computationally intensive we rely on a quasi-static energy based model of the grasp, a common approach when analyzing slow moving hands [39, 40]. In this model, the object is fixed in space relative to the hand and the interaction between the hand and object is modeled as a frictionless contact at each tangent point between a link and the object. Based upon these simplifications, the grasp model predicts the contact and reaction forces exerted on the object for a given applied tendon force. By sampling a grid of possible object positions relative to the hand, we are then able to predict where valid grasps exist and how the object will reconfigure as well as evaluate the general performance of the hand for the particular object.

To model the behavior of the hand when grasping we rely on the Freeform Manipulator Analysis Toolbox, a set of tools developed to analyze serial manipulator mechanisms [41]. The serial kinematics of each digit of the hand, couplings between

various joints, elastic elements, and frictionless contacts with the object are represented in terms of homogeneous transformations between the related elements. Elastic elements and applied forces and torques (such as the actuator force) are expressed in terms of their contribution to the system energy.

The total energy of the system in a given configuration can then be calculated based on the energy stored in elastic elements and the mechanical work done by the actuation inputs from the joints' zero position to the particular configuration. System constraints such as contact between the object and fingers are expressed in terms of homogeneous transforms that can be evaluated for a given hand configuration. The hand configuration that minimizes the energy function while respecting the distance constraints enforced via nonlinear equality and inequality constraint functions can then be found using the nonlinear multivariable solver (MatLab `fmincon` function). Conveniently, the routine we use solves for the minimum using the method of Lagrange multipliers: the minimum of function  $f(x)$  subject to constraints  $g(x) = 0$  may be found by solving the function  $\nabla f(x) = \lambda \nabla g(x)$ . Since  $\nabla f(x)$  corresponds to the joint forces and torques and  $\nabla g(x)$  corresponds to the constraint Jacobian, this expression is equivalent to  $F = \lambda J'$  so  $\lambda$  corresponds to the contact forces required to satisfy the position constraints. Although the solver is capable of approximation the gradient functions, since they can be explicitly computed by the toolbox they are also passed to the solver as well.

## PERFORMANCE METRICS

Here we evaluate the robustness of grasps via the following metrics: the maximum inward force exerted on the object, the maximum mechanical work performed on the object moving from the edge of the grasp to equilibrium, the minimum total normal force exerted on the object, and the portion of the hand's workspace where an inward force is exerted on the object. Since these metrics are force based, all designs are evaluated when actuated with the same input force and the results are normalized by this force. The performance can then be thought of in terms of the grasp efficiency.

For the maximum inward force metric, we report the maximum reaction force exerted on the object for a particular object hand pair. Practically, the inward reaction force corresponds to either the maximum weight or outward force that could be applied to the object before it could be pulled out of the grasp for the given actuator input. Maximizing this parameter results in a hand design that can grasp the heaviest object or resist the largest constant disturbance force for a given actuator force.

Although a continuously applied force greater than the maximum inward force could clearly pull an object out of the grasp, if the force is only exerted briefly, such as when the object is struck or bumps into the environment, the object may only shift in the grasp. Therefore, we also compute the work required to overcome the reaction force applied to the object by the hand as the object is moved from its equilibrium position within the hand to the edge of the hand's workspace.

Maximizing this parameter in turn increases the magnitude of the outward impulse that the hand can resist.

Although the model does not include contact friction, the maximum frictional shear forces that can be resisted at each contact will be proportional to the normal forces. Therefore, maximizing the normal forces serves as a proxy for frictional forces the grasp can exert. The minimum normal force metric is computed by summing all of the individual contact normal forces for each valid object position and reporting the smallest total normal force that the hand exerts. Maximizing this parameter and ensuring that the normal force is never zero will ensure that the resulting design is robust to some amount of out of plane disturbance forces.

Lastly, we want to evaluate the positional error tolerance of the hand since the ability to precisely position the hand relative to the object is not guaranteed. To quantify this aspect of the hand's performance, we calculate the area of possible initial object positions relative to the hand where the hand exerts an inward force on the object. Although objects may still be grasped outside of this region (when no reaction force is exerted on the object it can still be pinched between the fingertips), in these cases the grasp will rely entirely on the friction forces to resist disturbances and therefore will not be very robust. Finally, in some cases, the reaction force may push the object out of the hand, clearly an undesirable result.

## RESULTS AND DISCUSSION

Based upon this overall hand morphology and modeling approach, we investigate the impact of hand parameters including link lengths, revolute joint moment arms, and object sizes on the performance of the hand. To do so, we evaluate a range of possible hand configurations grasping various diameter cylindrical objects using this model and metrics. To simplify comparison of different designs, we have chosen to normalize all dimensions by the length of a single finger (from base to tip). Therefore, the total length of a finger including the proximal intermediate and distal phalanges is equal to 1 in all cases and phalange lengths and object radii are expressed in fractions thereof. Similarly, the distal phalanx's pulley moment arm is expressed as a fraction of the distal phalanx's length while the intermediate phalanx's moment arm is expressed as a fraction of the sum of the lengths of the intermediate and distal phalanx. Lastly, all hand configurations are evaluated grasping a range of objects with radii from 0.1 to 0.5 times the length of the finger.

We begin by investigating the impact of the relative link lengths on the hand. Specifically, for a hand with intermediate and distal joint torques of  $0.9(\ell_1 + \ell_2)$  and  $0.9\ell_2$  times the proximal joint force, we vary the length of the intermediate phalanx ( $\ell_1$ ) from 0 to 0.45 and the distal phalanx ( $\ell_2$ ) from 0 to 0.9. For each configuration, the length of the proximal phalanx ( $\ell_b$ ) equals  $1 - (\ell_1 + \ell_2)$ . This can result in a negative proximal phalanx length which corresponds to the intermediate phalange joint being located behind the palm. The impact of these parameters on the hand's performance as quantified by the inward force, work, and normal force metrics as a function of

object size is shown in Figure 4. We have also condensed the simulation results across object diameters by averaging the normalized results as shown in Figure 5. As can be seen in these contour plots, an optimal region exists for each metric and object size. For smaller objects, the inward force and work based metrics favor a long distal link and short proximal link and as the object diameter increases the model predicts that a hand with a longer proximal link and shorter distal link will perform best. A similar trend, with the optimum shifted slightly, favoring even longer intermediate and distal links can be seen for the normal force metric.

The first column of Figure 4 shows the hands' performance based on the inward force metric. The subplots show that there is an optimal link length region for each object diameter (marked with a black dot) and that as the grasped object diameter increases, the optimal distal link length decreases and the impact of the intermediate link length decreases. Although this is not directly shown in the plot, this behavior is a direct result of how the phalanx lengths and moment arms are defined. The joint moment arms are defined as a fraction of the link length distal to them. Therefore, increasing the link lengths increases the joint moment arms and joint torques applied by the tendon, and the maximum force applied to the object. However, since the total finger length is fixed equal to 1, increasing the intermediate and distal link lengths, shortens the proximal link length. Since the object cannot penetrate the palm, shortening the proximal link length reduces how far around the object the fingers can wrap and the maximum inward force they exert. This relationship manifests itself in the shifting optimal region that balances increasing the intermediate and distal link lengths as proxies for the joint moment arms while ensuring sufficient proximal phalanx length to wrap about the object. A similar optimal region stemming from the same set of factors can be seen in the second column of Figure 4 as expected since this metric is simply the integral of the inward force over all possible object positions.

The third column of Figure 4 shows the impact of the link lengths on the minimum of the sum of the normal forces exerted on the object by the hand. These plots all show a region of constant minimum normal force for shorter link lengths. The size of this region shrinks as the object diameter increases. The link lengths within this region correspond to hand designs where the proximal link length is long enough that for some object positions, the object only contacts the proximal links when the revolute joints reach their travel limits. The region where the minimum normal force is highest is adjacent to the region of constant normal force since this corresponds to hand designs where the revolute joints of the fingers have almost reached their travel limits when the object contacts the palm, thereby maximizing finger wrap and the number of contacts for the object position corresponding to the minimum normal force.

Figure 5 shows the average performance of the hand on these three metrics over the range of object diameters. In this figure, the performance of each hand for each size object is normalized by the performance of the optimal design and then

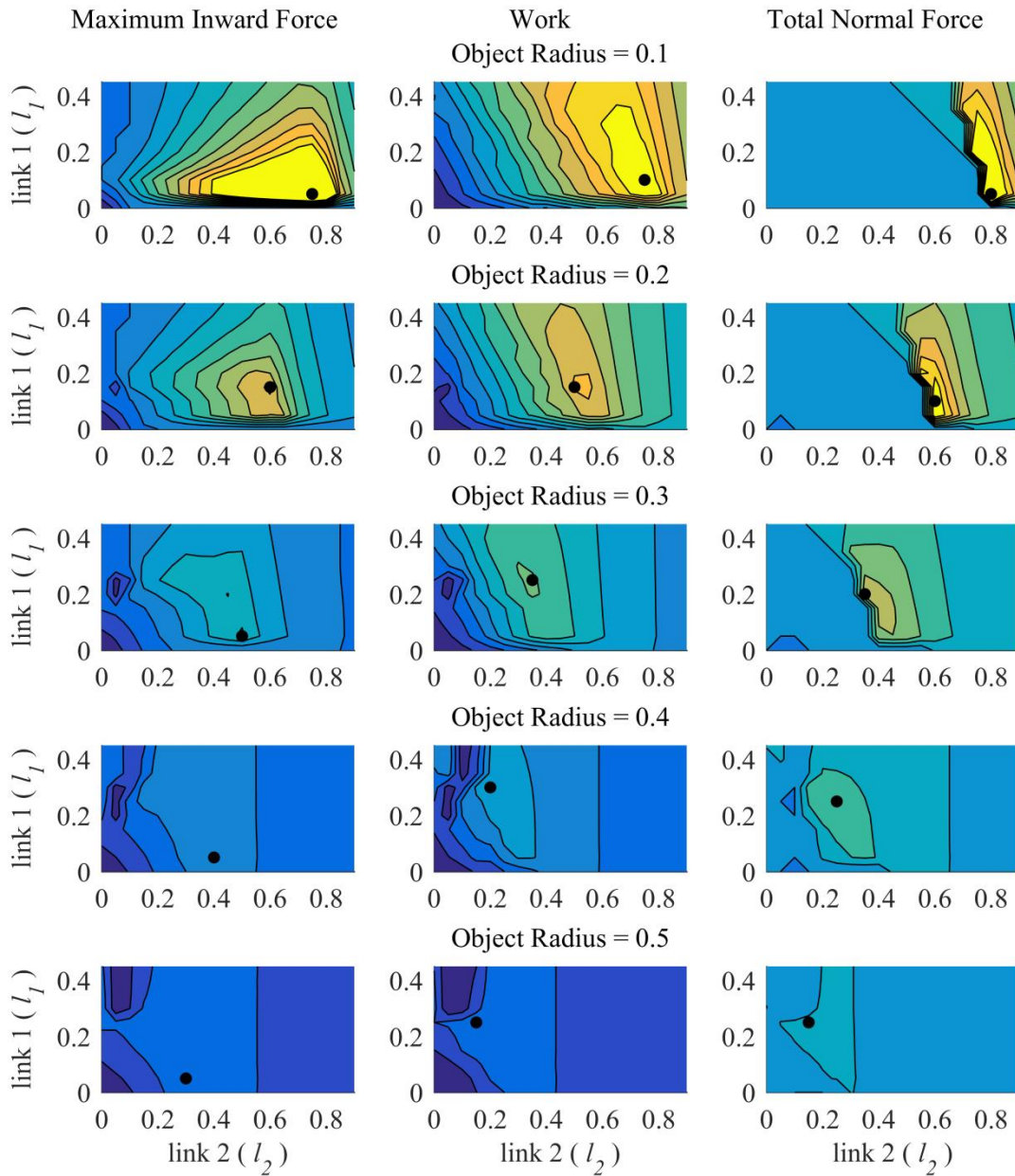


**Figure 4. Impact of link lengths on the performance of the hand design. Joint moment arms are fixed at 0.9 times the respective links as described in the methods above. Each row shows the performance of the hand as characterized by the inward force (column one), work (column two) and total normal force (column three) metrics when the link lengths are varied. Maxima for each metric and object are marked on the contour plots with a black dot.**

the results for all of the object sizes are averaged. This means that normalized performance for each diameter and overall average performance will be between zero and one and ensures that the performance for each size object is weighted equally. As can be seen in the first subplot, based on the inward force metric, there is a very clear optimum where the intermediate link is 0.07 and the distal link is 0.5 times the overall finger length. The work based metric shows a large optimal region with intermediate link lengths from 0.15 to 0.45 and distal link lengths from 0.35 to 0.45 with performance increasing slightly for a shorter intermediate and longer distal link lengths. Lastly,

there isn't a clear trend in the right most subplot that shows the average performance on the total normal force metric. Instead there appears to be a number of nearly vertical optimal regions corresponding to the bands for each diameter object which do not overlap.

Based upon these results, we believe that a hand design with a distal link of approximately 0.5 to 0.6, an intermediate link of 0.2 to 0.3 and proximal link of 0.1 to 0.3 balances the performance on all three metrics across a wide range of object diameters. As can be seen in Figures 4 and 5, link lengths in this range fall near the maxima for the inward force and work

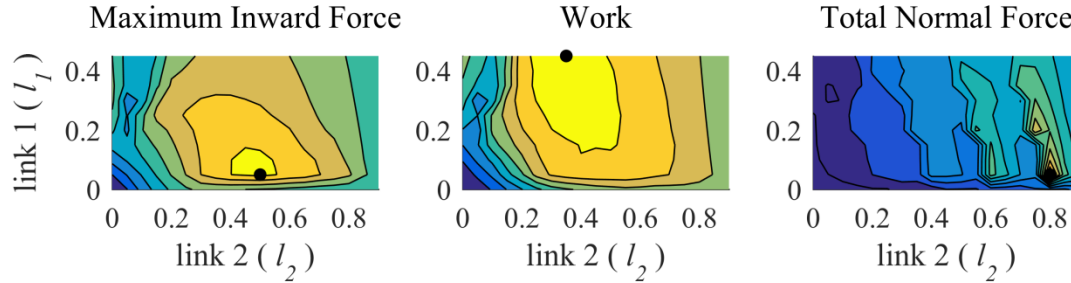


**Figure 5. Average performance over all simulated object diameters. The optimization results for each diameter were normalized by their respective maxima and all the results were averaged for each metric.**

metrics for all of the object diameters that we analyzed. Although these link lengths do not fall near the total normal force optimum across all object diameters, optimizing for this metric is difficult because the optimal region for this metric is smaller than for the other two and moves from one extreme to the other across the full range of object diameters. Therefore, this set of link lengths represents a reasonable compromise since it results in good performance on all three metrics for average (0.2 – 0.3) radius objects and acceptable performance for smaller and larger objects.

Next, we vary the joint moment arms while fixing the link lengths based on the previous optimization results to investigate the impact of the revolute joint moment arms on the hand’s performance. For this simulation, we selected an intermediate phalanx length equal to 0.24 and a distal phalanx length of 0.58. We then varied both the intermediate and distal joint torque ratios ( $r_1$  and  $r_2$ ) from 0 to 2 times the length of the finger distal to the respective joints and simulated the resulting hand grasping cylindrical objects with radii from 0.1 to 0.5 times the total finger length. We show the impact these parameters have on the hand’s performance as measured by the maximum inward force, work, and grasp area metrics in Figure 6. As can be seen in these plots, increasing either or both of the moment arms from zero improves the hand’s performance on the inward force metric for all object sizes we tested. For smaller objects, the work metric also increases continuously with moment arm but for larger objects, it is maximal when the moment arms equal 1. Lastly, the grasp area is maximized regardless of object diameter when either moment arm equals 1. The average performance across object radii is shown in Figure 7. This figure clearly summarizes these trends: the inward force metric increases with moment arm length, the work based metric shows a clear optimum when both moment arms are about 1, and the grasp area is maximized when either equals one.

The relationship between maximum inward force and moment arm shown in the first column of Figure 6 makes intuitive sense: for a given hand object configuration, increasing the moment arm will increase the joint torques and resulting contact forces on the object. However as can be seen in these figures, when one moment arm is much longer than the other, further increasing it has no effect on the hand’s performance. This is because the longer moment arm causes the associated joint to reach its travel limit before the maximum

object force is exerted.

Like the results for the force based metric, increasing the length of either or both moment arms improves the hand’s performance as measured by the work based metric as shown in column two of Figure 6. However, the impact of the moment arms varies somewhat with their relative lengths. When both moment arms are less than one, increasing the length of either or both improves the hand’s performance. When one moment arm is shorter than one and the other is longer than one, changes in performance are primarily effected by changes in the moment arm that is shorter than one. This is because the difference in moment arm lengths results in the joint with the moment arm greater than one flexing until it reaches its hard stop, at which point further increases in the moment arm will have no effect. Lastly, when both moment arms are greater than one, performance increases for small objects but not for larger objects. Although the longer moment arms increase the magnitude of the contact forces and work done on the object for smaller objects, for larger objects, it also reduces how far around the object the fingers can wrap before it contacts the palm, reducing the range of object positions that are valid.

The grasp area metric is maximized when either moment arm equals one. This is because this metric is effectively measuring the equilibrium point of the hand: if the moment arms equal one, the fingers will start to exert an inward force when the object is at the fingertip, resulting in the hand pulling the object further into the hand from the edge of the workspace. If the moment arms are less than one, the fingers will not start to cage inward until the object moves further into the grasp, reducing the portion of the workspace where the object is drawn into the grasp. Lastly, if the moment arms are greater than one, the fingers will cage inward and eject the object when it makes contact near the tip, resulting in a smaller set of valid grasps that draw the object in.

These results are summarized in Figure 7 where the average performance across tested object sizes is plotted for the three metrics. For each object diameter the performance of all configurations is normalized by the performance of the optimal design and then the results are averaged across object diameters. This summation of the results shows how joint moment arms of length one optimize the performance of the design across object diameters for all three metrics.

Based upon these results, we believe that a design with joint moment arms equal to one maximize the hand’s overall

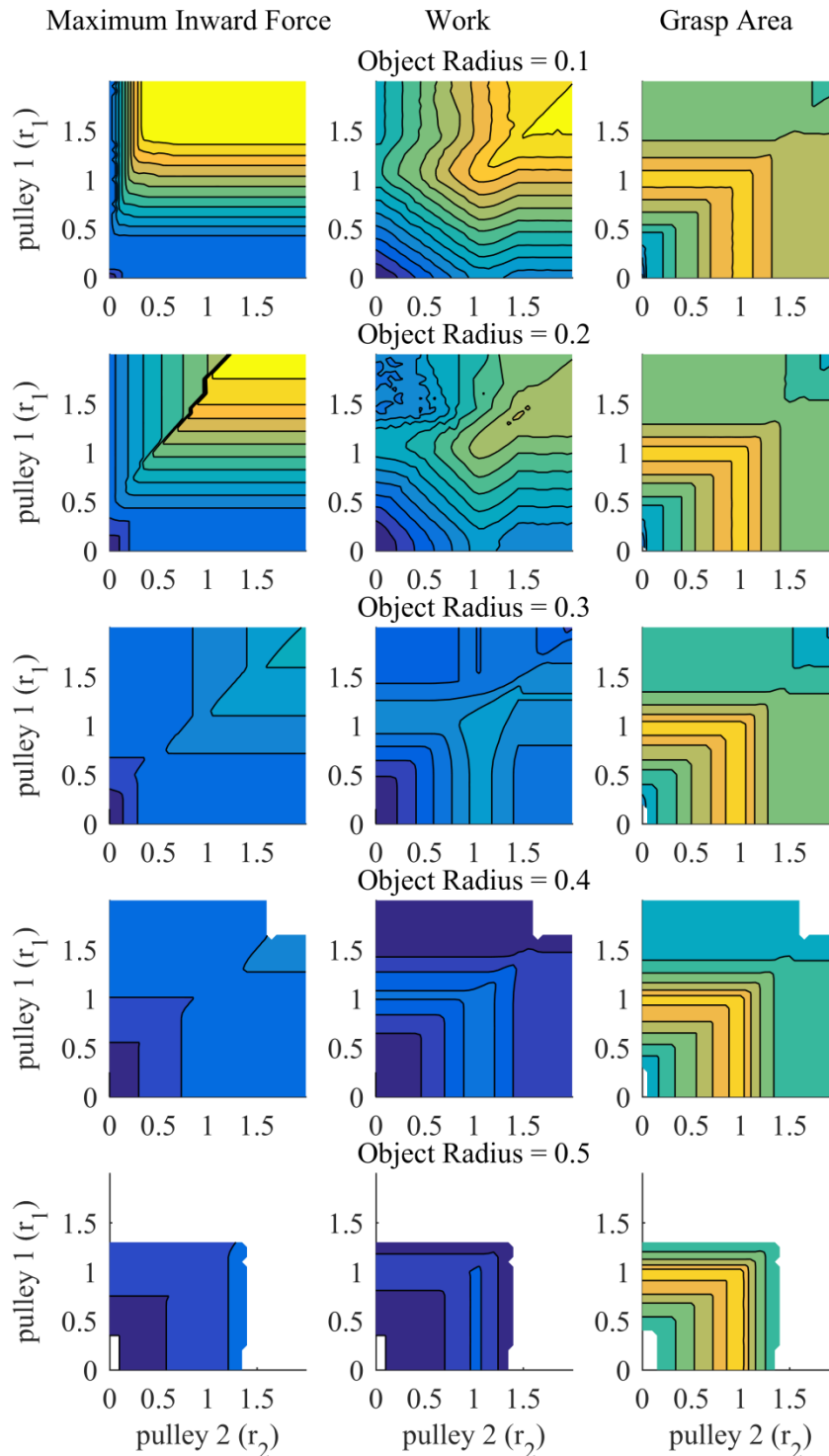
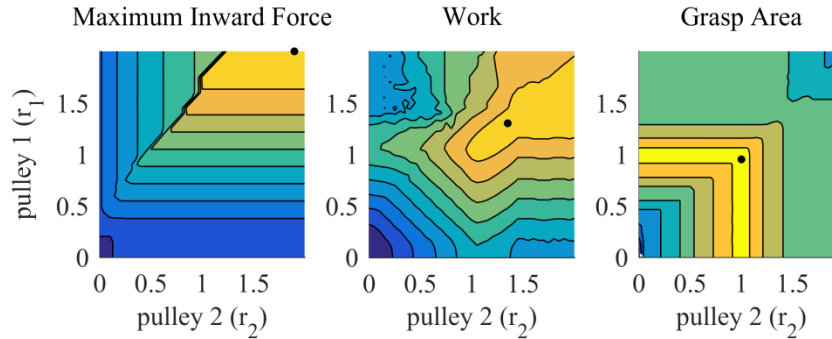


Figure 6. Impact of joint moment arms on the performance of a hand with intermediate phalanx lengths of 0.24 and distal phalanx lengths of 0.58. Each row shows the performance of the hand as characterized by the inward force (column one), work (column two) and total normal force (column three) metrics when the joint moment arms are varied for a give object radius. Regions of the plots where the model fails to find a valid solution are left blank.



**Figure 7. Impact of joint moment radii on the average performance over all simulated object diameters. The optimization results for each diameter were normalized by their respective maxima and all the results were averaged for each metric**

performance on the work and grasp area metrics across all object diameters. Although longer moment arms would increase the performance on the maximum inward force metric, this relationship is unbounded so there is no clear optima. Instead designing based on this metric is limited based upon the physical constraints of the hand as well as the hand ejecting the object as the moment arm increases further.

### CONCLUSIONS AND FUTURE WORK

Here we presented the model and analysis of the grasping performance of a prismatic-revolute-revolute joint hand and investigate the impact of the link lengths and joint moment arms on its general grasping performance and use as an aerial grasper. This analysis showed that a hand with these kinematics and a distal link length of approximately 0.5 to 0.6, an intermediate link length of 0.2 to 0.3, a proximal link length of 0.1 to 0.3, and joint moment arms equal to the total digit length distal to the respective joints maximizes the hands overall performance over a wide range of object sizes.

In follow-on work, we will build and test a new hand based upon these optimization results that incorporates the P-R-R joint finger configuration and optimized link lengths and moment arms discussed here. This prototype and experimental evaluation of the design will help validate the behaviors predicted by the model and demonstrate the general grasping capabilities of a hand based on the P-R-R finger morphology.

### ACKNOWLEDGMENTS

This work was funded in part by the National Science Foundation, grant IIS-1317976.

### REFERENCES

[1] The Shadow Robot Company, 2015, "Shadow Dexterous Hand," <http://www.shadowrobot.com/products/dexterous-hand/>.

[2] Grebenstein, M. et al., 2011, "The DLR hand arm system," Proc. IEEE International Conference on Robotics and Automation (ICRA), pp. 3175-3182.

[3] Birglen, L., Gosselin, C., and Laliberté, T., 2008, "Underactuated Robotic Hands," Springer tracts in advanced robotics., Springer-Verlag Berlin Heidelberg., Berlin, Heidelberg.

[4] Odhner, L. U. et al., 2014, "A compliant, underactuated hand for robust manipulation," The International Journal of Robotics Research, 33(5), pp. 736-752.

[5] Mason, M. T., Rodriguez, A., Srinivasa, S. S., and Vazquez, A. S., 2012, "Autonomous manipulation with a general-purpose simple hand," The International Journal of Robotics Research, 31(5), pp. 688-703.

[6] Ciocarlie, M. et al., 2014, "The Velo gripper: A versatile single-actuator design for enveloping, parallel and fingertip grasps," The International Journal of Robotics Research, 33(5), pp. 753-767.

[7] Ulrich, N., Paul, R., and Bajcsy, R., 1988, "A medium-complexity compliant end effector," Proc. Proceedings of the IEEE International Conference on Robotics and Automation, pp. 434-436 vol.431.

[8] Robotiq, 2015, "Adaptive Robot Gripper," <http://robotiq.com/products/industrial-robot-hand/>.

[9] Leutenegger, S. et al., 2016, "Flying Robots," Springer Handbook of Robotics, B. Siciliano, and O. Khatib, eds., Springer International Publishing, Cham, pp. 623-670.

[10] Roderick, W. R. T., Cutkosky, M. R., and Lentink, D., 2016, "Touchdown to take-off: at the interface of flight and surface locomotion," Interface Focus, 7(1).

[11] Google X, 2016, "Project Wing," <https://x.company/projects/wing/>

[12] Amazon.com, 2016, "Amazon Prime Air," <https://www.amazon.com/Amazon-Prime-Air/b?ie=UTF8&node=8037720011>.

[13] Deutsche Post Group, 2016, "DHL Parcelcopter 3.0," [http://www.dpdhl.com/en/media\\_relations/specials/parcelcopter.html](http://www.dpdhl.com/en/media_relations/specials/parcelcopter.html).

[14] Desbiens, A. L., Asbeck, A. T., and Cutkosky, M. R., 2011, "Landing, perching and taking off from vertical surfaces," The International Journal of Robotics Research, 30(3), pp. 355-370.

[15] Mellinger, D., Shomin, M., Michael, N., and Kumar, V., 2013, "Cooperative grasping and transport using multiple quadrotors," Distributed autonomous robotic systems, Springer, pp. 545-558.

[16] Graule, M. A. et al., 2016, "Perching and takeoff of a robotic insect on overhangs using switchable electrostatic adhesion," Science, 352(6288), pp. 978-982.

[17] Hawkes, E. W., Jiang, H., and Cutkosky, M. R., 2016,

- "Three-dimensional dynamic surface grasping with dry adhesion," *The International Journal of Robotics Research*, 35(8), pp. 943-958.
- [18] Yanagimura, K., Ohno, K., Okada, Y., Takeuchi, E., and Tadokoro, S., 2014 "Hovering of MAV by using magnetic adhesion and winch mechanisms," *Proc. IEEE International Conference on Robotics and Automation (ICRA)*, pp. 6250-6257.
- [19] Kessens, C. C., Thomas, J., Desai, J. P., and Kumar, V., 2016, "Versatile aerial grasping using self-sealing suction," *Proc. IEEE International Conference on Robotics and Automation (ICRA)*, pp. 3249-3254.
- [20] Gawel, A. et al., 2016, "Aerial Picking and Delivery of Magnetic Objects with MAVs," *arXiv preprint arXiv:1612.02606*.
- [21] Pope, M. T. et al., 2016, "A Multimodal Robot for Perching and Climbing on Vertical Outdoor Surfaces," *IEEE Transactions on Robotics*, PP(99), pp. 1-11.
- [22] Lindsey, Q., Mellinger, D., and Kumar, V., "Construction of cubic structures with quadrotor teams," *Proc. Robotics: Science & Systems VII*.
- [23] Willmann, J., Augugliaro, F., Cadalbert, T., D'Andrea, R., Gramazio, F., and Kohler, M., 2012, "Aerial Robotic Construction Towards a New Field of Architectural Research," *International Journal of Architectural Computing*, 10(3), pp. 439-460.
- [24] Augugliaro, F., et al., 2014, "The Flight Assembled Architecture installation: Cooperative construction with flying machines," *IEEE Control Systems*, 34(4), pp. 46-64.
- [25] Korpela, C., Orsag, M., and Oh, P., 2014, "Towards valve turning using a dual-arm aerial manipulator," *Proc. IEEE/RSJ International Conference on Intelligent Robots and Systems*, pp. 3411-3416.
- [26] Pounds, P. E. I., Bersak, D. R., and Dollar, A. M., 2011, "Grasping from the air: Hovering capture and load stability," *Proc. IEEE International Conference on Robotics and Automation (ICRA)*, pp. 2491-2498.
- [27] Doyle, C. E., et al., 2013, "An Avian-Inspired Passive Mechanism for Quadrotor Perching," *IEEE/ASME Transactions on Mechatronics*, 18(2), pp. 506-517.
- [28] Thomas, J., Loianno, G., Daniilidis, K., and Kumar, V., 2016, "Visual Servoing of Quadrotors for Perching by Hanging From Cylindrical Objects," *IEEE Robotics and Automation Letters*, 1(1), pp. 57-64.
- [29] Chi, W., Low, K. H., Hoon, K. H., and Tang, J., 2014, "An optimized perching mechanism for autonomous perching with a quadrotor," *Proc. IEEE International Conference on Robotics and Automation (ICRA)*, pp. 3109-3115.
- [30] Suseong, K., Seungwon, C., and Kim, H. J., 2013, "Aerial manipulation using a quadrotor with a two DOF robotic arm," *Proc. IEEE/RSJ International Conference on Intelligent Robots and Systems (IROS)*, pp. 4990-4995.
- [31] Thomas, J., Polin, J., Sreenath, K., and Kumar, V., 2013, "Avian-Inspired Grasping for Quadrotor Micro UAVs," *International Design Engineering Technical Conferences & Computers and Information in Engineering Conference (IDETC/CIE) Portland, OR*.
- [32] Huber, F., et al., 2013, "First analysis and experiments in aerial manipulation using fully actuated redundant robot arm," *Proc. IEEE/RSJ International Conference on Intelligent Robots and Systems*, pp. 3452-3457.
- [33] Kim, S., Hoseong, S., and Kim, H. J., 2015, "Operating an unknown drawer using an aerial manipulator," *Proc. IEEE International Conference on Robotics and Automation (ICRA)*, pp. 5503-5508.
- [34] Kondak, K., et al., 2014, "Aerial manipulation robot composed of an autonomous helicopter and a 7 degrees of freedom industrial manipulator," *Proc. IEEE International Conference on Robotics and Automation (ICRA)*, pp. 2107-2112.
- [35] Cano, R., Pérez, C., Pruano, F., Ollero, A., and Heredia, G., 2013, "Mechanical Design of a 6-DOF Aerial Manipulator for assembling bar structures using UAVs," *Proc. Workshop on Research, Education and Development of Unmanned Aerial Systems*.
- [36] Backus, S. B., and Dollar, A. M., 2016, "An Adaptive Three-Fingered Prismatic Gripper With Passive Rotational Joints," *IEEE Robotics and Automation Letters*, 1(2), pp. 668-675.
- [37] Backus, S. B., Odhner, L. U., and Dollar, A. M., 2014, "Design of Hands for Aerial Manipulation: Actuator Number and Routing for Grasping and Perching," *IEEE/RSJ International Conference on Intelligent Robots and Systems (IROS) Chicago, IL*.
- [38] Lyons, D. M., 1985, "A simple set of grasps for a dextrous hand," *Proc. Proc. IEEE International Conference on Robotics and Automation*, pp. 588-593.
- [39] Aukes, D. M., and Cutkosky, M. R., 2013, "Simulation-based tools for evaluating underactuated hand designs," *Proc. IEEE International Conference on Robotics and Automation (ICRA)*, pp. 2067-2073.
- [40] Mason, M. T., and Salisbury Jr, J. K., 1985, *Robot hands and the mechanics of manipulation*, MIT Press.
- [41] Odhner, L., and Dollar, A., 2010, "The Freeform Manipulator Analysis Tool," <https://www.eng.yale.edu/grablab/fmat/>.